THE ASTROPHYSICAL JOURNAL, 329:498–510, 1988 June 1

LABORATORY STUDIES OF THE INFRARED SPECTRAL PROPERTIES OF CO IN ASTROPHYSICAL ICES

S. A. SANDFORD, L. J. ALLAMANDOLA, A. G. G. M. TIELENS,[1] AND G. J. VALERO
NASA/Ames Research Center
Received 1987 August 18; accepted 1987 November 25

ABSTRACT

Analysis of laboratory spectra of numerous astrophysical ice analogs demonstrates that the exact band position, width, and profile of the solid state CO fundamental near 2137 cm^{-1} (4.679 μm) can provide important information on the physical conditions present during the ice accretion phase as well as during any subsequent thermal processes and radiation exposure. In the ices studied, the CO peak position varies from 2134 to 2144 cm^{-1} (4.686 to 4.664 μm) and the band width from 2.1 to over 20 cm^{-1} depending on the composition of the ice. In an ice matrix dominated by H_2O, the CO peak falls at 2136.7 cm^{-1}, has a full width at half-maximum of about 9 cm^{-1}, and shows a prominent sideband at 2152 cm^{-1}. This sideband and minor structure superposed on the main band arise from CO trapped in different matrix sites. These features provide information concerning the thermal and radiation history of the ice.

The solid CO band in interstellar spectra often has contributions from broad (12 cm^{-1}) and narrow (5 cm^{-1}) components. We identify the broad component with CO intimately mixed in matrices dominated by polar molecules, of which H_2O is likely to be the major component. Examination of the interstellar and laboratory band profiles shows that either the abundance of nonpolar impurities in these ices must be less than 10% or the ices have been thermally annealed or processed by ultraviolet radiation. The narrow component is likely to originate from grain mantles dominated by nonpolar molecules such as CO_2. These components reflect differences in the physical and chemical conditions in regions of the cloud along the line of sight.

Laboratory determination of the absorption strength of the CO fundamental in H_2O–rich ices showed that the value used in the past was approximately 60% too low and that most previously determined solid-state CO column densities have been systematically overestimated. The rich spectral behavior of the CO band observed in the laboratory studies clearly indicates that future high-quality astronomical spectra in the 2200–2100 cm^{-1} range can produce a wealth of new information and provide deeper insights into the nature of astrophysical ices.

Subject headings: infrared: spectra — laboratory spectra — line identifications — molecular processes — interstellar: grains — interstellar: molecules — interstellar: abundances

I. INTRODUCTION

Since the discovery of carbon monoxide in the interstellar medium by Wilson, Jefferts, and Penzias in 1971, gas-phase CO has been found to be both abundant and ubiquitous in interstellar space. Because CO is a stable molecule, it is present in a wide variety of objects and has become an important diagnostic of conditions in these objects (see van Dishoek 1987, and references therein). The important role CO plays in interstellar chemistry has also become widely recognized during the last decade (see, for example, Tarafdar and Vardya 1987). Despite the widespread use of CO as a probe of physical conditions of interstellar gas, its equally important role as a diagnostic of conditions in interstellar ices, as well as its importance in revealing many of the chemical and physical properties of interstellar and cometary ices, has not been fully appreciated.

In 1980, Hagen, Allamandola, and Greenberg pointed out that CO in the solid phase absorbs near 2140 cm^{-1} (4.67 μm), and they suggested a search for the solid CO feature in the spectra of infrared sources embedded in molecular clouds. Although absorption near this position had been found by Soifer *et al.* (1979) in the spectrum of W33 A, the spectral resolution and peak position precluded a definite assignment to solid CO. The first unambiguous identification of this band was made by Lacy *et al.* (1984), an observation which has been confirmed by Larson *et al.* (1985). Whittet, Longmore, and McFadzean (1985) have found this feature in the spectra of several regions of the Taurus dark cloud complex. Most recently, Geballe (1986) has extended these observations and found the solid CO signature in many well-known obscured infrared objects. Of the 27 embedded sources for which spectra have been measured in this wavelength range, 16 have the solid CO feature. In several cases the amount of CO in the solid phase is comparable to the amount of CO present in the gas.

In addition to allowing one to determine the column density of CO frozen in grain mantles, the solid CO band profile and position can be used to provide insight into the composition and thermal history of interstellar ices. Although there have been many infrared spectroscopic studies of CO in solids at very low temperatures, few of the solids examined to date are pertinent to CO in astrophysical ices. The infrared spectra of pure CO films (Ewing and Pimentel 1961; Legay-Sommaire and Legay 1982) and CO in rare gas matrices (Dubost 1976; Dubost and Abouaf-Marguin 1972; Jiang, Person, and Brown 1975) have been investigated in detail. However, only a few studies have examined ice mixtures containing CO (e.g., Hagen, Tielens, and Greenberg 1983; Kitta and Kratschmer 1983), and these have not focused on the spectral properties of the CO fundamental.

[1] Also Space Sciences Laboratory, UC Berkeley.

To expand the data base on which astronomical observations and models must rely, we have measured the infrared spectroscopic and condensation-vaporization properties of CO in pure and mixed ices. In this paper we present the spectral properties of CO in various ices. These include peak positions, full widths at half-maxima (FWHM), band profiles, and integrated absorbances (band strengths) of the CO fundamental at 2137 cm^{-1} in different ices under various conditions. It is shown that good quality, moderate-resolution spectra of the interstellar CO feature can be used to unravel the composition, concentration, temperature, and thermal history of interstellar and cometary ices containing CO. In a separate paper we report the results of an extensive series of experiments on the condensation and vaporization properties of CO and CO–H_2O ices determined by using the infrared properties described here (Sandford and Allamandola 1988). Binding energies, diffusion coefficients, and related parameters are presented in the second paper.

II. EXPERIMENTAL PROCEDURES

Only a brief summary of the procedures used will be given here as a detailed description of the experimental equipment and techniques will be presented in a forthcoming paper (Allamandola, Sandford, and Valero 1988).

All the gas mixtures were prepared in a greaseless, glass vacuum system designed to allow for careful control of the concentrations of molecules mixed in each sample bulb. All liquids used (purity greater than 99.5%) were further purified by three freeze-thaw cycles under vacuum, while gases (purity greater than 99.5%) were taken directly from gas cylinders and used without further purification. After allowing ample time for complete mixing, the gas samples were slowly condensed onto a cold CsI window suspended in a vacuum chamber. Depositions were made at pressures of $\sim 5 \times 10^{-8}$ millibar. The flow of gas onto the CsI window was regulated by a microflowmeter, and samples were typically deposited at a rate of 1.6×10^{-5} moles per hr. This corresponds to a thickness growth rate of 5 μm per hr. The window temperature was controlled by a closed-cycle helium refrigerator. By using a resistive heater mounted on the window holder, the temperature of the CsI window could be maintained at any point between 10 and 280 K. The temperature was measured with an absolute accuracy of ± 2 K and a relative accuracy of ± 0.2 K with an Fe-Au/Chromel thermocouple placed in a small hole inside the window mounting. The resistive heater could be controlled in such a manner as to allow for sample warm-up or cool-down at predetermined rates. The CsI window is rotatable. Besides facing the deposition port, the window can be turned toward a microwave-powered, hydrogen discharge lamp which simulates the interstellar ultraviolet radiation field. The window can also be rotated to line up with the beam axis of a Fourier transform infrared spectrometer.

Infrared transmission spectra were measured from 4000 to 400 cm^{-1} (2.5–25 μm). The resolution of the spectrometer was determined to be 0.9 cm^{-1} (the observed width of an unresolved line). Spectral positions are accurate to ± 0.2 cm^{-1} because of oversampling.

III. RESULTS AND DISCUSSION

In this section the peak positions, full widths at half-maxima (FWHM), band shapes, and integrated absorbances of the ^{12}CO fundamental near 2140 cm^{-1} (4.67 μm) and the ^{13}CO fundamental near 2090 cm^{-1} (4.78 μm) will be discussed. The data presented represent the synthesis of over 210 spectra involving experiments on over 55 ice mixtures. Before presenting the results, it is appropriate to briefly review the effects and interactions that lead to band shifting and broadening when molecules are in the solid state. A more detailed discussion of these effects can be found elsewhere (Allamandola 1984; Tielens and Allamandola 1987*b*, and references therein).

The fundamental vibration of a molecule suspended in a solid matrix will be shifted from the gas-phase frequency due to interactions with the surrounding molecules. These interactions can be chemical or physical. Chemical interactions generally involve the transfer of electrons. Since the highest filled molecular orbital in CO is nonbonding, while the next orbital is antibonding and empty, formation of a molecular complex which involves electrons donated to the CO will weaken the bond, resulting in a shift to lower frequency. Any complex that withdraws electrons from the CO will tend to have little or no effect on the fundamental frequency unless substantial withdrawal occurs (cf. Huheey 1983). Physical interactions include attractive contributions from electrostatic (dipole and quadrupole), inductive (dipole-induced dipole), and dispersive (London) forces as well as repulsive forces (electron cloud overlap) between the guest species and neighboring molecules of the matrix (Barnes 1973). Thus, the physical interaction can depend on the size and shape of the site, the distribution of the surrounding species, and the dielectric constant, dipole moment, and polarizability of the matrix molecules. If the overall interaction is attractive (repulsive) the peak position shifts to lower (higher) frequencies with respect to the gas phase values. Since the net interaction is the combined effect of many different terms which differ from one matrix to another, no simple relation is expected between measured spectral quantities and individual physical parameters of the matrix molecules.

When species are deposited at temperatures much lower than their melting point, an amorphous, rather than crystalline structure is produced. This is because each individual molecule is quickly "frozen" into place in a substitutional (replacing a host molecule) or interstitial (in-between host molecules) site. As there is insufficient energy at these low temperatures to permit rearrangement to occur, a solid is produced in which the lattice is highly disordered. Thus an amorphous ice has a wider distribution of molecular environments than a crystalline solid. This results in the production of relatively broad, Gaussian-like band profiles such as those shown for CO in Figure 1. Upon warming, the molecules in these ices rearrange themselves into more energetically favorable orientations, and somewhat more ordered amorphous structures are produced. This process, called annealing, usually produces sharper bands because the range of different environments is reduced. Warming to a sufficiently high temperature (about 130 K in the case of H_2O ice) will eventually result in the production of a crystalline structure with regular spacings and orientations of the individual molecules (see Tielens and Allamandola 1987*a* for further discussion of this kinetic transformation).

Typically, the main solid CO peak only falls a few wavenumbers to the red of the gas phase value (see below). This implies either (i) CO forms a very weak complex with the matrix molecules, which is essentially similar in all cases, or (ii) the site is always slightly larger than the CO molecule and its electron cloud. In the latter case, dispersive interactions between the electrons in the matrix material and the CO molecule attract the carbon and oxygen, producing a redshift. In the matrices studied here, physical interactions dominate over chemical

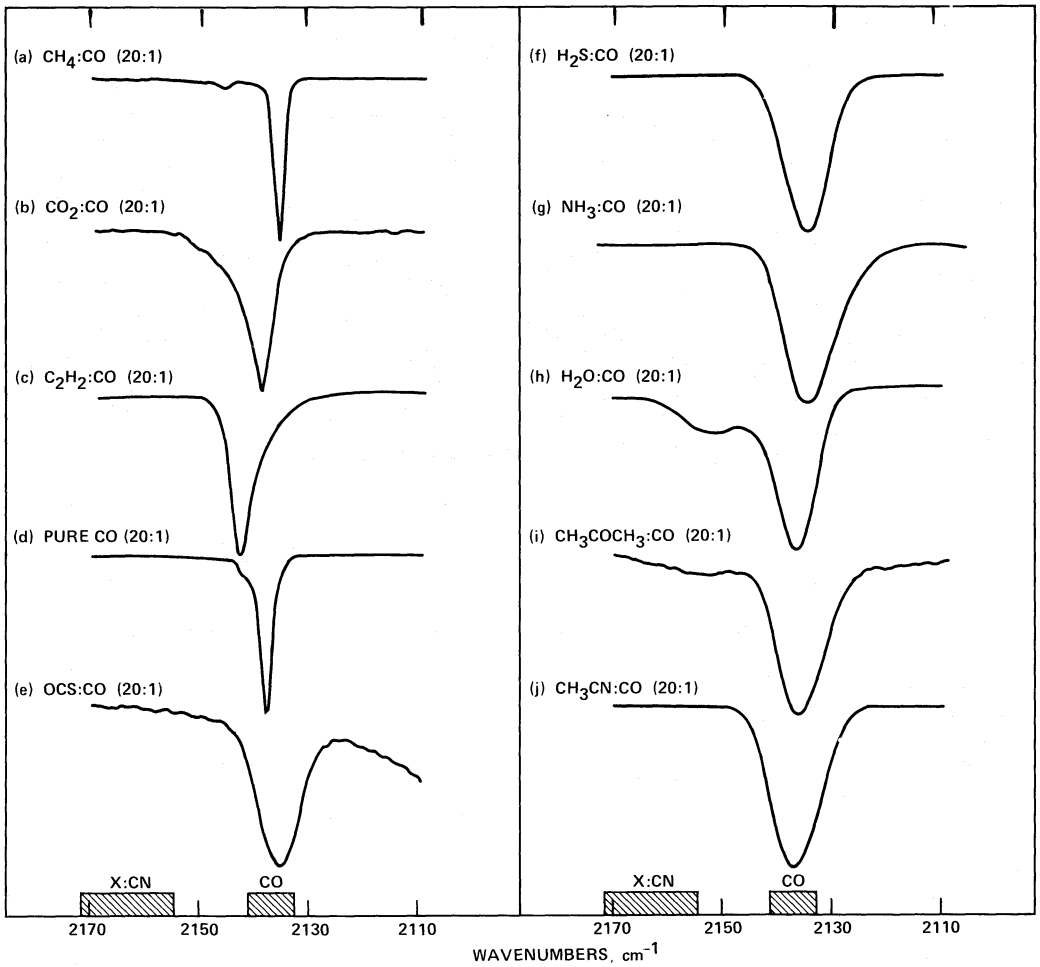

FIG. 1.—The band profile of the C≡O stretching fundamental of CO suspended in ices comprised of molecules with dipole moments that span the range from 0 to 3.9 debye. The dipole moment of the matrix material increases from spectrum (*a*) to spectrum (*j*). The ice:CO ratio of 20:1 is representative of the concentration of CO in interstellar ices. The cross-hatched areas at the bottom of the figure indicate the typical position and FWHM of the interstellar CO and *X*(CN) features. All the spectra presented in this paper were taken at a resolution of 0.9 cm^{-1}. Note the prominent feature at 2152 cm^{-1} in the H_2O:CO ice spectrum due to a second major matrix site (see text). The small feature at 2145.5 cm^{-1} in the CH_4:CO spectrum is probably due to minor contamination by H_2O (see Dubost [1976] for a discussion of the infrared properties of CO binary complexes). Also note that the weak, broad band near 2153 cm^{-1} in the CH_3COCH_3:CO spectrum is due to acetone and not to a second site.

interactions because the site size only varies a little between the different matrix materials used, while the ability of the various constituents to donate or withdraw electrons varies widely.

a) ^{12}CO *Peak Position and Profile*

While the FWHM for pure CO ice lies between 1.0 and 2.5 cm^{-1}, depending on its degree of crystallinity, the width of this band in astrophysical spectra is usually much larger (Lacy *et al.* 1984; Whittet, Longmore, and McFadzean 1985; Geballe 1986). In the work presented here, spectra of CO frozen in different icy matrices were measured to ascertain how the peak position, FWHM, profile, and strength of the CO stretching vibration near 2137 cm^{-1} depends on the nature of the ice. The observed CO band parameters for the different ice matrices are summarized in Table 1. Figure 1 shows the CO fundamental band as it appears when the CO is incorporated into these ice matrices at 10 K. In all but the pure CO ice case, the ratio of matrix material to CO was 20:1. This ratio was chosen as it is similar to the ratio found in many interstellar ices (Tielens and Allamandola 1987*b*).

The peak position showed little variation in these experiments and fell between 2134.5 and 2143.9 cm^{-1} (see Table 1). The CO band peaks at 2136.7 cm^{-1} when the CO is trapped in H_2O–rich ices. As expected, although there is a general trend in the behavior of the CO peak position and FWHM with such physical parameters as dipole moment, polarizability, and refractive index of the host matrix material, there is no simple relationship (see, for example, Fig. 2). Except for the case of CO in acetylene, the CO band is slightly redshifted in the binary ice mixtures relative to the 2143 cm^{-1} fundamental frequency of gas-phase CO, implying that the attractive terms in the interaction dominate.

The FWHM we observe for pure CO ice is larger than the values of 1.0 to 1.5 cm^{-1} reported for films above 20 K (Ewing and Pimental 1961; Legay-Sommaire and Legay 1982). At these higher temperatures the CO is expected to be in the α-phase and more crystalline than the amorphous CO ice that is produced at 10 K. Our interpretation that the broader bandwidth in pure CO ice is due to its more amorphous nature is supported by the observation that the FWHM decreases from 2.5 cm^{-1} to 2.0 cm^{-1} as the CO ice is warmed from 10 K to 30 K at a rate of 2 K per minute. Similar widths were measured

TABLE 1

THE SPECTRAL PROPERTIES OF CO IN VARIOUS ICE MIXTURES

Ice Composition	Matrix Dipole Moment (debye)	CO Peak (cm^{-1})	CO FWHM[a] (cm^{-1})	CO Shoulder Position (cm^{-1})	Shoulder[b] / Main
CO	0.12	2138.6	2.5	2142.5[c]	...
CO film on H_2O	0.12	2138.7	2.5	...	...
CH_4:CO = 20:1	0.00	2136.5	2.2	2145.5[c]	...
+UV	0.00	2136.8	3.5	...	...
O_2:CO = 20:1	0.00	2136.3	2.7	...	...
+UV	0.00	2136.4	5.5	...	...
CO_2:CO = 20:1	0.00	2139.7	5.8	...	...
C_2H_2:CO = 20:1	0.00	2143.9	4.6	...	...
OCS:CO = 20:1	0.67	2135.7	8.8	...	...
H_2S:CO = 20:1	1.00	2134.5	7.9	...	...
+UV	1.00	2134.6	9.6	...	...
NH_3:CO = 20:1	1.47	2137.1	10.9	...	...
H_2O:CO = 20:1	1.80	2136.7	8.8–9.3	2151.7	0.26
+UV	1.80	2136.3	9.6	2152.0	0.10
H_2O:CO = 140:1	1.80	2136.5	8.4	2154.0	0.25
H_2O:CO = 1:10	0.12	2138.7	3.4	...	...
CH_3COCH_3:CO = 20:1	2.90	2136.4	9.9	2152.7[d]	0.17
CH_3CN:CO = 20:1	3.92	2137.2	10.4	...	...
+UV	3.92	2136.6	10.9	...	...
H_2O:CO:CH_4 = 20:1:2	...	2136.3	10.4	2151.7	0.58
+UV	...	2136.2	9.8	2150.2	0.35
H_2O:CO:C_3H_8 = 20:1:2	...	2136.2	23.5	2150.0	0.72
H_2O:CO:C_3H_8 = 20:1:0.1	...	2136.5	8.8	2152.5	0.27
H_2O:CO:C_6H_{14} = 20:1:2	...	2136.0	23.1	2148.0	0.75
+UV	...	2136.0	11.9	2149.4	0.39
H_2O:CO:C_8H_{18} = 20:1:2	...	2136.7	22.2	2147.4	0.71
+UV	...	2135.7	14.7	2147.3	0.55
H_2O:CO:CH_3OH = 20:1:2	...	2136.5	9.4	2152.4	0.16
H_2O:CO:$(CH_3)_2CO$ = 20:1:2	...	2137.2	10.5	2151.9	0.15
H_2O:CO:NH_3 = 100:2:1	...	2137.1	9.6	2153.0	0.31
H_2O:CH_3OH:CO:NH_3 = 100:50:1:1	...	2136.4	10.3	2152.1	0.25
H_2O:CH_3OH:CO:NH_3 = 100:50:1:10	...	2136.5	10.2	2152.0	0.20

[a] Measured on percent transmission spectra.
[b] Ratio of integrated band intensities.
[c] CO–H_2O dimer complex.
[d] Acetone mode.

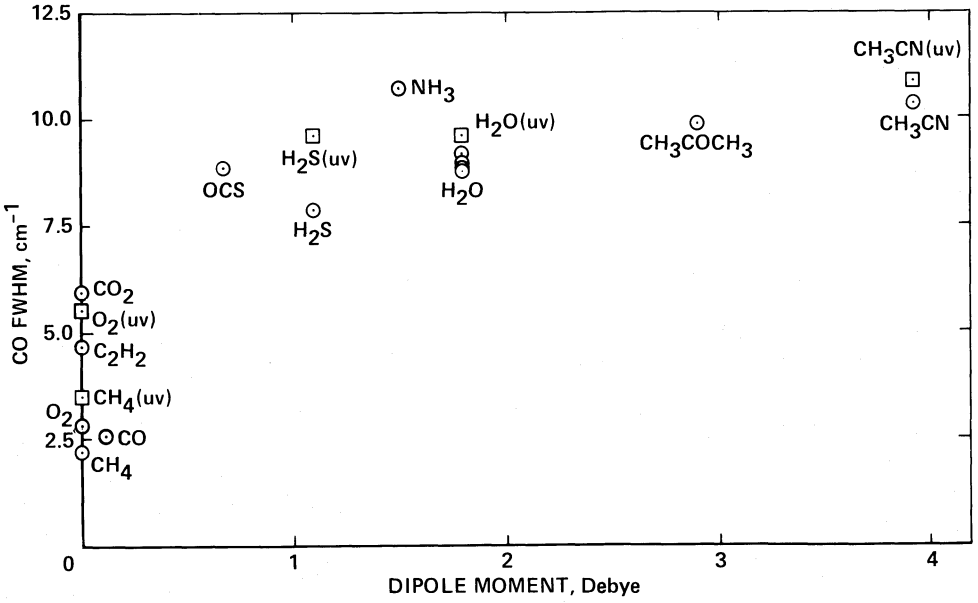

FIG. 2.—The FWHM of the fundamental band of CO vs. the dipole moment of the embedding matrix molecules. The circles represent values taken from unprocessed ices while the squares represent values after 1–2 hr of ultraviolet photolysis. The values from four independent experiments using an unprocessed H_2O matrix are shown to indicate the extent of experimental variation. Each set of points is labeled with the identity of the matrix material.

when a thin film of CO was deposited at 10 K on top of a preexisting H_2O ice layer.

Realistic astrophysical ices will, of course, be more complicated than the simple binary mixtures discussed above. As part of another series of experiments (Allamandola, Sandford, and Valero 1988) we have also examined the spectra of CO in more complex ices which also contain CH_3OH and NH_3. The CO band in the spectra of these ices showed similar behavior to that described above. A summary of the results of these experiments is included in Table 1.

Since astrophysical ices containing CO are expected to be exposed to ultraviolet photons and cosmic rays which can lead to dissociation reactions and increased matrix disorder, several of the ice mixtures shown in Figure 1 were photolyzed for 1 to 2 hours. In Figure 2 the FWHM of the CO band in unphotolyzed ices are denoted by circles, those in photolyzed ices by squares. Photolysis increases the FWHM of the band by 0.5 to 2.7 cm^{-1} in these cases. The increase in FWHM upon photolysis presumably results from the increased disorder of the lattice structure due to the creation of lattice defects and photolysis products in substitutional and interstitial sites. Since photoinduced reactions are dependent on the optical properties of the matrix material, the amount of increase in FWHM is probably strongly influenced by photochemical effects that are matrix dependent. Exposure to ultraviolet radiation did not appreciably alter the peak position of the CO feature, although it did eliminate the 2152 cm^{-1} satellite band which is present when the CO is incorporated in water ices. This point will be discussed in more detail later.

Since H_2O–rich ices containing CO are expected to be formed under a variety of physical conditions in the interstellar medium and in comets, a series of depositions were carried out at temperatures of 10, 20, 30, 40, and 50 K for the H_2O:CO = 20:1 ices in order to investigate the effect of deposition temperature on the CO fundamental. Each of these samples was subsequently warmed in steps at a rate of 2 K per minute to higher temperatures of 20, 30, 40, 50, 65, 80, 100, 125, and 150 K, and the peak positions and FWHM of the CO band were monitored while the temperature was held constant at these values. Depositions above 65 K were not done since CO did not stick in H_2O matrices above this temperature under our laboratory conditions. Similarly, warm-up experiments were not done above 150 K since H_2O ices sublime rapidly above this temperature at our low laboratory pressures. Figure 3 contains plots of the CO fundamental for an H_2O:CO (20:1) ice that was deposited at 10 K and subsequently warmed to the temperatures listed above. Figure 3 and Table 2 show that the CO peak position steadily shifts to lower frequencies as the temperature increases from 10 to 150 K. At 10 K the main band is at 2136.7 cm^{-1} and it shifts monotonically down to 2134.4 cm^{-1} by 150 K. In addition, as the amorphous H_2O ice is warmed, the H_2O molecules rearrange into a somewhat more ordered amorphous structure. This annealing process apparently produces a family of new sites in the water ice at about 100 K, as evidenced by the appearance of new absorption features at 2135.9 and 2143.6 cm^{-1} (weak). The presence of these bands on the short wavelength side of the original CO band suggests that they are due to CO held in less attractive sites. These new features could possibly be related to the formation of clathrate-like structures. Both features increase in strength relative to the original band as the temperature is increased from 100 to 150 K.

The FWHM of the CO fundamental initially decreases as the ice is warmed from 10 K to about 100 K, after which it apparently begins to increase again (see Fig. 4 and Table 2). The behavior below 100 K can be understood in terms of the annealing of the water ice. The increasing order of the H_2O molecules in the matrix during warm-up gives rise to a decreasing range in the physical sites available to be occupied by the CO, resulting in a narrower CO band. Blending of the original

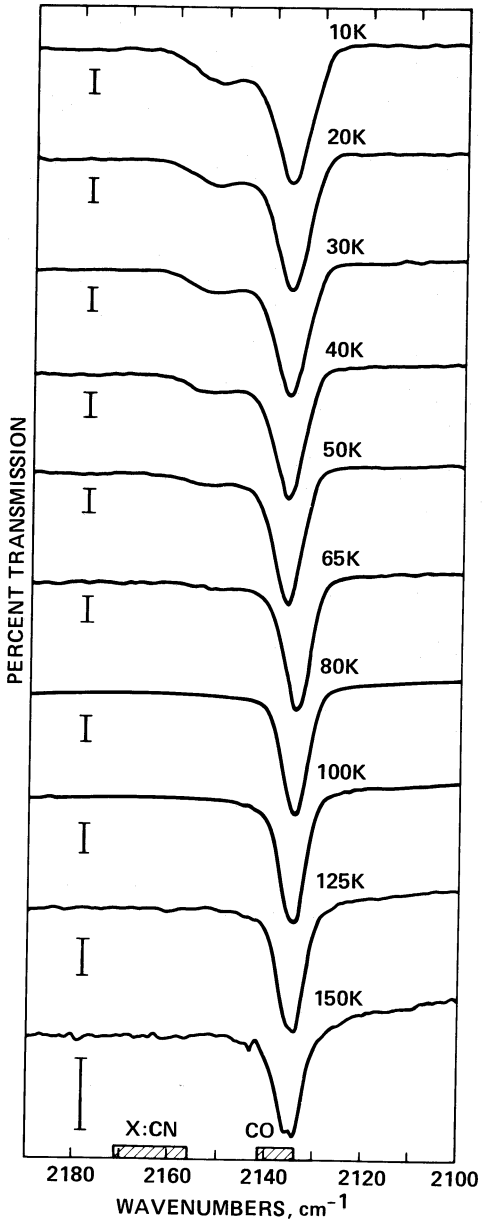

FIG. 3.—Spectra demonstrating the change in position and profile of the CO fundamental band in an H_2O: CO = 20:1 ice mixture as it is warmed from 10 to 150 K. The warm-up rate between temperature steps was 2 K per minute and spectra were taken while the temperature was held fixed for 20 minutes. The bar displayed with each spectrum denotes 1% transmission. Note that (i) the 2152 cm^{-1} shoulder decreases with warm-up and is gone by 80 K, (ii) the original fundamental band shifts steadily from 2136.7 cm^{-1} to 2134.4 cm^{-1} as the sample is warmed from 10 to 150 K, and (iii) new bands appear at 2134.6 and 2135.9 cm^{-1} at 100 K and grow progressively stronger as the ice warms further. The cross-hatched areas at the bottom of the figure indicate the typical position and FWHM of the interstellar CO and *X*(CN) features.

TABLE 2

THE PEAK POSITION AND AVERAGE FWHM OF THE CO SOLID-STATE BAND VERSUS TEMPERATURE IN H_2O:CO = 20:1 ICES

Temperature (K)	Peak Position (cm^{-1})[a]	FWHM (cm^{-1})[a]
10	2136.7 ± 0.2	9.0 ± 0.2
20	2136.3	8.5
30	2136.1	8.0
40	2135.9	7.6
50	2135.8	7.0
65	2135.6	6.8
80	2135.2	6.6
100	2134.9[b]	6.4
125	2134.6[b]	6.6
150	2134.4[b]	7.0

[a] These values represent the average of several experiments, seven at 10 K, one at 20 K, two at 30 K, three at 40 K, and four each at 50, 65, 80, 100, 125, and 150 K.

[b] New features appear near 2136 cm^{-1} and 2144 cm^{-1} upon warming to 100 K. The peak position listed here is that of the initial CO fundamental peak.

(shifted) CO band with the new 2135.9 cm^{-1} feature that appears at 100 K causes the apparent FWHM to increase again as the temperature rises above 100 K.

Note from Figure 4 that the FWHM of the CO fundamental band is slightly narrower and the peak position slightly shifted at any given temperature for ices deposited at higher temperatures. This is the result of the kinetics of the annealing process. In order for a molecule to change orientation during annealing it must overcome an energy activation barrier corresponding to the bulk binding energy of the ice ($\Delta H_v/k \sim 7900$ K for H_2O). During deposition, however, some anealing can occur at the surface where the activation barrier is related to the lower, surface binding energy ($\Delta H_s/k \sim 4900$ K, see Sandford and Allamandola 1988, and references therein). Consequently, an H_2O matrix that is deposited at a low temperature and subsequently annealed at a higher temperature will be less ordered than an H_2O matrix directly deposited at that higher temperature.

b) The 2152 cm^{-1} Side Band in H_2O Matrices

A shoulder centered near 2152 cm^{-1} (4.647 μm) was observed in all binary ice mixtures in which water was the major matrix material. This feature does not appear prominently in any of the spectra taken of CO in the other materials. The integrated absorption strength of the shoulder relative to the main CO band was observed to be about 0.26. This shoulder is attributed to a second CO trapping site which is unique to amorphous water ice. The fact that the shoulder is shifted to a frequency higher than the gas-phase CO fundamental position (i.e., is "blueshifted") implies that repulsive interactions dominate over attractive ones. Thus, we attribute the main CO peak at 2136.7 cm^{-1} to CO substituting for an H_2O molecule in the ice matrix, and the 2152 cm^{-1} shoulder to interstitial CO located within the pores of the amorphous H_2O lattice. Presumably the CO molecules are being frozen into the water matrix during deposition into one of two major types of sites, with the sites responsible for the 2152 cm^{-1} band containing about 20% of the total CO.

To better understand the source of the 2151 cm^{-1} shoulder a number of additional experiments were carried out in which H_2O water was the main component of the matrix. First, an additional experiment was done in which the H_2O:CO ratio was increased from 20:1 to 140:1 (i.e., lower CO concentration). The shoulder-to-main peak ratio for this run was found to be 0.25; i.e., unchanged from the higher concentration experiments. This implies that the shoulder is not due to CO-CO interactions since the fraction of CO molecules frozen as part of a CO dimer in the low concentration experiment (0.014) is negligible compared to the fraction (0.18) in the high concentration experiments (Behringer 1958). Likewise, it is not due to CO·$(H_2O)_n$ complexes which also absorb near this frequency (Hagen and Tielens 1981).

Second, experiments were performed in which the structure of the H_2O ice was systematically perturbed by the presence of various hydrocarbons. Initially, the mixtures H_2O:CO:X = 20:1:2, where X was CH_4 (methane), C_3H_8 (propane), C_6H_{14} (hexane), and C_8H_{18} (octane), were used. The spectra of these

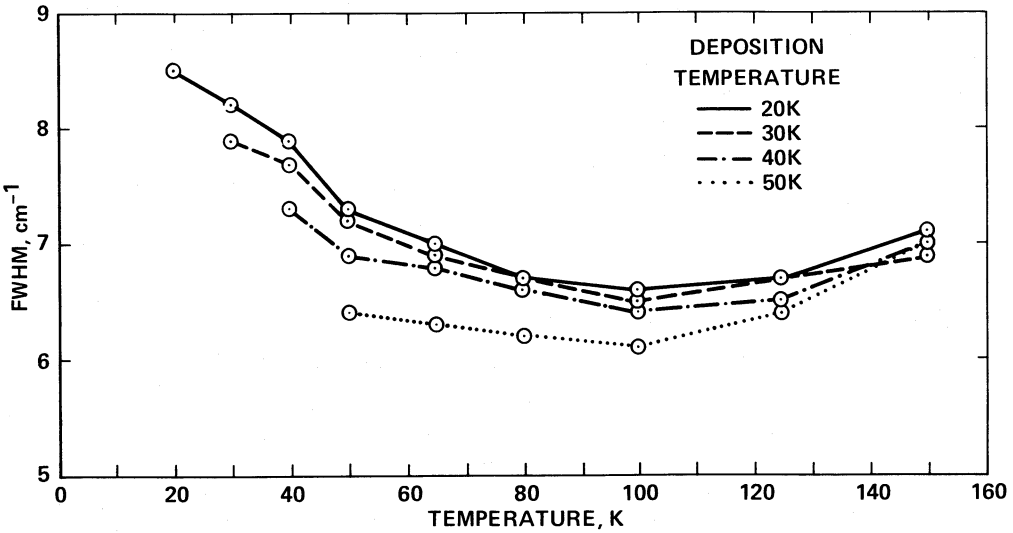

FIG. 4.—The FWHM of the CO fundamental band as a function of temperature and thermal history. The curves trace the FWHM observed in individual H_2O:CO = 20:1 ices deposited at 20, 30, 40, and 50 K and subsequently warmed in steps to 150 K. Note that (i) the FWHM decreases when the ice is warmed to 100 K and thereafter apparently begins to increase, and (ii) ices deposited at higher temperatures tend to have FWHM that are systematically smaller than ices deposited at lower temperatures which are subsequently warmed to the same temperature.

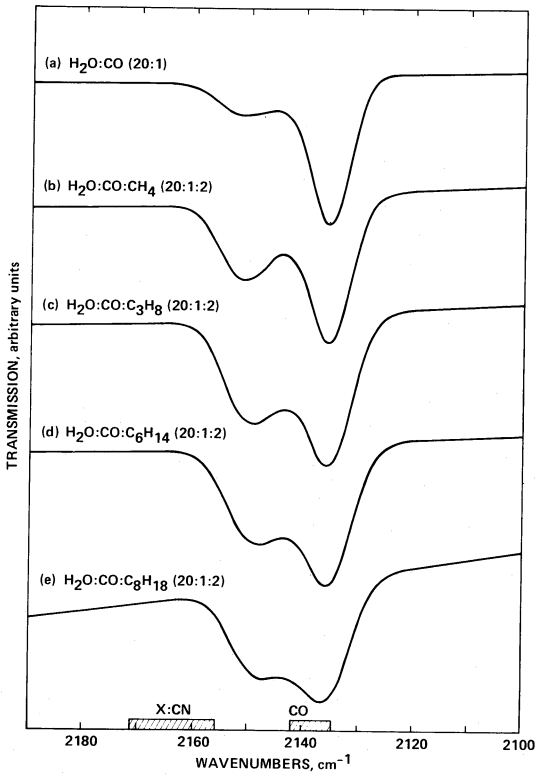

FIG. 5.—The 2190–2100 cm^{-1} spectra of the fundamental band of CO frozen in H_2O:CO: X = 20:1:2 ice mixtures where $X = CH_4$ (methane), C_3H_8 (propane), C_6H_{14} (hexane), and C_8H_{18} (octane). Note the increasing relative strength of the 2152 cm^{-1} shoulder as the molecular size of the hydrocarbon "contaminant" increases. The cross-hatched areas at the bottom of the figure indicate the typical position and FWHM of the interstellar CO and X(CN) features.

samples are shown in Figure 5. The resulting shoulder-to-main band intensity ratios for samples containing methane, propane, hexane, and octane are 0.58, 0.72, 0.75, and 0.71, respectively. Clearly the introduction of a high concentration of nonpolar hydrocarbon contaminants into the H_2O matrix increases the number of interstitial (2152 cm^{-1}) CO trapping sites over that found in ices containing only H_2O and CO. The spectrum of the mixture H_2O:CO:C_3H_8 = 20:1:0.1 (not shown) has a shoulder-to-main intensity ratio of about 0.27 (the same as in water ices without any hydrocarbons), showing that the effect is concentration-dependent. In the mixtures H_2O:CO:CH_3OH = 20:1:2 and H_2O:CO:$(CH_3)_2CO$ = 20:1:2 the shoulder-to-main intensity ratio was not enhanced above that normally seen in H_2O-rich ices. Apparently hydrocarbon impurities with hydrogen-bonding capabilities will not disorder the H_2O hydrogen-bonding network as much as nonpolar impurities and create fewer interstitial sites.

Third, upon warm-up the amorphous H_2O structure anneals and the number of interstitial sites should be reduced. In fact, the relative absorption contribution from the shoulder does decrease as H_2O:CO = 20:1 ices are warmed up (cf. Fig. 3). The shoulder-to-main ratios for warm-up from 10 K to 20, 30, 40, 50, 65, 80, and 100 K for this ice are 0.26, 0.21, 0.22, 0.20, 0.17, 0.11, 0.06, and less than 0.05, respectively. The relative contribution of the shoulder is smaller in H_2O:CO ices that are deposited at higher temperatures. Similarly, during warm-up of an H_2O:CO:C_3H_8 = 20:1:2 ice to these same temperatures, the shoulder-to-main intensity ratio changed from 0.78 to 0.80, 0.66, 0.64, 0.57, 0.39, 0.22, and 0.14. Note that CO is lost from both types of site during the warm-up process but at different rates. It is therefore not clear what fraction of the interstitial CO moved into substitutional sites and what fraction escaped the matrix altogether.

Finally, the behavior of the 2152 cm^{-1} shoulder after ultraviolet photolysis is of interest. The relative strength of the shoulder decreases rapidly with exposure to ultraviolet radiation. This is true for both the H_2O:CO experiment shown in Figure 1 and the H_2O:CO:X experiments shown in Figure 5. Again, observation of the individual band areas showed that CO was being lost from both sites but was being lost from the interstitial sites at a much higher rate. When an ultraviolet photon is absorbed in the water ice, its energy will initially be deposited in a small volume within the matrix promoting local molecular rearrangement or photochemistry or both. Molecular rearrangement should preferentially produce a loss of CO molecules from the repulsive (2152 cm^{-1}) sites. Photochemistry involving CO molecules trapped in the repulsive site should also be enhanced since the CO molecules in this site interact more strongly with the H_2O molecules in the matrix.

Thus all the available data suggest that amorphous water ice traps CO in two major types of sites. The site responsible for the 2152 cm^{-1} band is less stable and is only significantly populated in amorphous H_2O–rich ices that have not been annealed by thermal warm-up above 80 K and have not been substantially processed by ionizing radiation.

c) ^{13}CO *Peak Position and Profile*

In the experiments with the stronger CO bands and good signal-to-noise ratio it was possible to measure the ^{13}CO fundamental absorption band. In pure CO this band falls at 2092.5 cm^{-1} (4.790 μm). In water matrices the ^{13}CO fundamental falls between 2089 and 2090 cm^{-1} (4.787 and 4.785 μm). As with the ^{12}CO band, the presence of surrounding matrix molecules (not just H_2O) lowers the frequency of the band slightly with respect to the gas-phase peak position. The FWHM of the ^{13}CO band is similar to that of the ^{12}CO band.

The strength of the ^{13}CO fundamental relative to the ^{12}CO band was observed to vary between 0.011 and 0.014. This variation is largely due to experimental uncertainty related to the lower signal-to-noise ratio of the ^{13}CO features. This ratio is consistent with the terrestrial $^{13}C/^{12}C$ ratio of 0.0112 and implies that the integrated band strength for solid ^{13}CO is the same as that of ^{12}CO.

d) *Integrated Band Intensity and Column Density*

The column density N (molecules cm^{-2}) of an infrared band carrier can be determined using the equation

$$N = \frac{\int \tau_\nu \, d\nu}{A} \approx \frac{\tau_{max} \Delta\nu_{1/2}}{A} \qquad (1)$$

where τ_{max} is the optical depth of the band at maximum absorbance, $\Delta\nu_{1/2}$ is the FWHM of the band (measured in absorbance) in cm^{-1}, and A is the absorption intensity of the band in centimeters per molecule. There are often large infrared intensity differences between vibrational transitions of a molecule in the gas phase and those same vibrations when the molecule is in the solid phase. Similar differences can also be produced when the molecule is placed in matrices with different compositions. Consequently, the column density of an individual component in an interstellar ice can only be accurately

determined using the A values measured in realistic ice analogs. However, only a limited number of pure and mixed ices of astrophysical interest have been studied (Bertie, Labbe, and Whalley 1969; Hagen, Tielens, and Greenberg 1981, 1983; Wood and Roux 1982; Leger *et al.* 1983; d'Hendecourt and Allamandola 1986). In view of the widespread occurrence of CO (and probably CO_2) frozen in H_2O–rich ices in the interstellar medium and comets, and in order to quantify the photolysis experiments discussed later in this paper, we have experimentally determined the A values of CO and CO_2 frozen in H_2O matrices.

Twelve carefully prepared mixtures of H_2O: CO (20:1) and one mixture of H_2O:CO_2 (20:1) were individually deposited using the techniques described earlier. No pressure rise was detected to a sensitivity of 3×10^{-9} millibar during any of these depositions, ensuring that the ratios of CO and CO_2 to H_2O in the ices were the same as in the original gas mixtures. Band saturation was avoided by integrating bands in samples for which the infrared peak absorption by the 3280 cm^{-1} O-H stretch band of the H_2O ice was less than 50%. The integrated strength of the OH stretch in amorphous ice is not affected by small (<30%) impurity concentrations (Hagen, Tielens, and Greenberg 1983). Using the A-value for amorphous solid water of $A(H_2O)_{3280} = 2.0 \times 10^{-16}$ cm molecule^{-1}, the number of water molecules in the infrared beam was calculated. The number of CO molecules was then determined using the initial H_2O:CO ratio, and the A(CO) value computed by solving equation (1) for A. A similar approach was used to determine the A-values for CO_2 in a water matrix. Our computed A-values, as well as those for H_2O ices, are listed in Table 3.

The A-value determined for CO in H_2O ice is 70% higher than that of pure CO. This is qualitatively consistent with the observations of Jiang, Person, and Brown (1975) who noted that, while the A-values of CO in solid CO and CO isolated in argon matrices were both near 1.0×10^{-17} cm molecule^{-1}, there was a small increase in the A-value when SF_6, CCl_4, and C_6H_6 matrices were used. Our derived value for CO in H_2O falls close to the values they report in these other matrices.

The new A-values derived for CO_2 are about a factor of 4 larger than those estimated previously by d'Hendecourt and Allamandola (1986). This difference is presumably due to saturation effects in the earlier work. The 2340 cm^{-1} band in their samples had optical depths close to unity. This is evidenced by the ratio of the $^{13}CO_2$ to $^{12}CO_2$ band strengths in their spectrum which is much larger than expected from the terrestrial isotopic ratio. Therefore, the A-values for CO_2 reported here are the better values.

e) *Photolyzed Ices Containing* CO

Ultraviolet photolysis of the ice mixtures examined in this work always resulted in the loss of some of the original CO with simultaneous growth of CO_2. Figure 6 shows the spectra of a simple H_2O:CO = 20:1 ice mixture before and after a 2 hr exposure to ultraviolet radiation. Note the loss of CO demonstrated by the decrease in the 2137 cm^{-1} band and the simultaneous production of CO_2 as shown by the appearance of the 2342 cm^{-1} (4.270 μm) C=O stretching and 653 cm^{-1} (15.3 μm) O=C=O bending mode bands of CO_2.

When the newly derived A-values were used with the data shown in Figure 6 to determine the CO conversion efficiency it was found that slightly more CO was lost than could be accounted for by the production of CO_2. This discrepancy is at least partially accounted for by CO consumed in the production of HCO and H_2CO (weak bands attributed to both of these species are present when the lower spectrum shown in Fig. 6 is expanded). Assuming all the photolyzing radiation striking the sample was absorbed, a comparison of the number of ultraviolet photons absorbed with the number of CO molecules lost shows that the photochemical conversion of CO in this particular H_2O–rich ice occurs with a quantum efficiency of approximately 3%.

IV. ASTROPHYSICAL APPLICATIONS

a) *Summary of Experimental Results*

The peak position and profile of the fundamental stretching vibration of solid CO depend on the interactions of the CO molecules with the surrounding icy matrix. The laboratory studies presented in § III show that the peak position and bandwidth depend on site geometry as well as on interactions with neighboring molecules. Ultraviolet photolysis and temperature variations have little effect on the band position. Ultraviolet photolysis slightly increases the FWHM of the 2137 cm^{-1} band from about 9 cm^{-1} in an H_2O–rich ice to about 10 cm^{-1}, while a rise in temperature decreases it to about 7 cm^{-1} (cf. Tables 1 and 2). In highly disordered, amorp-

TABLE 3

INFRARED BAND INTENSITIES

Molecule	Mode	Band Position cm^{-1} (μm)	A(cm molecule^{-1})
H_2O (pure)	O—H stretch	3280 (3.045)	2.0×10^{-16} [a]
H_2O (pure)	OH bend	1660 (6.024)	8.4×10^{-18} [b]
H_2O (pure)	libration	760 (13.16)	2.8×10^{-17} [b]
^{12}CO (pure CO)	C≡O stretch	2139 (4.675)	1.0×10^{-17} [c]
^{13}CO (pure CO)	C≡O stretch	2092 (4.780)	1.0×10^{-17} [d]
^{12}CO:H_2O (1:20)	C≡O stretch	2137 (4.680)	1.7×10^{-17} [d]
^{13}CO:H_2O (1:20)	C≡O stretch	2090 (4.785)	1.7×10^{-17} [d]
$^{12}CO_2$:H_2O (1:20)	C=O stretch	2342 (4.270)	2.1×10^{-16} [e]
$^{12}CO_2$:H_2O (1:20)	O=C=O bend	653 (15.31)	4.1×10^{-17} [e]

[a] Taken from Hagen, Tielens, and Greenberg 1981.
[b] Taken from d'Hendecourt and Allamandola 1986.
[c] Taken from Jiang, Person, and Brown 1975.
[d] This work. Values apply between 10 and 30 K.
[e] This work. These A-values are probably appropriate for $^{13}CO_2$ as well.

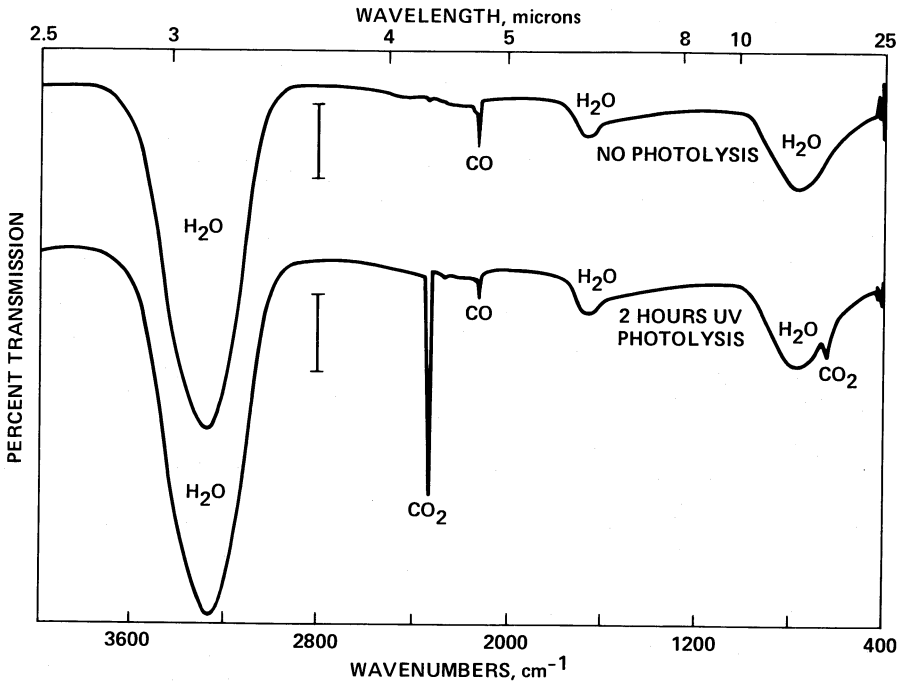

FIG. 6.—Spectra of an H_2O:CO = 20:1 ice mixture taken before (*top*) and after (*bottom*) 2 hr of ultraviolet photolysis. The bars represent 10% transmission. Note the decrease in the 2137 cm^{-1} CO band strength and the accompanying creation of solid-state CO_2 bands at 2342 and 653 cm^{-1}. While not obvious in the spectra plotted on this scale, small features attributed to HCO and H_2CO are also present in the photolyzed spectrum.

hous H_2O ice CO molecules can be trapped in two physically different type of sites: substitutional (CO replacing an H_2O molecule in the matrix) and interstitial (CO in the pores of the H_2O matrix). Because CO molecules in these different sites interact differently with neighboring molecules, they absorb at slightly different frequencies (2137 cm^{-1} versus 2152 cm^{-1}). In H_2O–rich ices deposited at 10 K these bands have relative absorption strengths of about 1 to 0.25. Upon warm-up, the ice matrix anneals and the effects of the interstitial sites become less pronounced (cf. Fig. 3). Above 80 K the 2152 cm^{-1} side band has completely disappeared. The 2152 cm^{-1} side band is even more pronounced when large, nonpolar (i.e. nonhydrogen bonding) impurity molecules are present in the H_2O ice. Even at low concentration levels ($\sim$10%), these impurities disrupt the hydrogen bonding network of the H_2O ice and give rise to a large number of the "interstitial" sites responsible for the 2152 cm^{-1} side band. When the disorder is large, the 2152 cm^{-1} band can become almost as strong as the 2137 cm^{-1} band resulting in the production of a composite, very broad CO absorption feature (cf. Fig. 5 and Table 1). The CO absorption bands in mixed molecular ices show a similar temperature dependence to that in pure H_2O (i.e., upon annealing the sideband disappears). It should be emphasized that hydrogen bonding impurities, such as CH_3OH, NH_3, and $(CH_3)_2CO$ can partake in the ice hydrogen bonding network and no enhancement of the 2152 cm^{-1} sideband is produced when these impurities are introduced into the H_2O ice (see the last five entries in Table 1).

b) *Observational Requirements*

Besides allowing one to determine the abundance of CO in astrophysical ices, astronomical observations of the solid-state CO band can also help constrain the environment of the CO molecules. However, the expected spectral variations characteristic of changes in the CO's environment are relatively small and observations with high spectral resolution ($\lambda/\Delta\lambda \sim 2000$) are required. High resolution is also needed to help disentangle the rovibrational lines of any gas-phase CO that may be along the line of sight. Gas-phase lines are seen toward many bright infrared objects embedded inside dense molecular clouds. Moreover, since the expected variations in the solid-state CO feature are generally small, high signal-to-noise ($\sim$100) studies are imperative. High signal-to-noise spectra will also be required if $^{13}C/^{12}C$ ratios are to be determined using the ^{13}CO and ^{12}CO bands at 2090 and 2137 cm^{-1}, the former of which is approximately 1/100 the strength of the latter.

In particular, careful observations of the peak position, width, profile, and presence (or absence) of the 2152 cm^{-1} shoulder and band splitting might be used as a thermometer to probe the thermal history of the ice mantle. Although the strength of the 2152 cm^{-1} band decreases upon ultraviolet photolysis, complicating the use of this thermometer somewhat, the effects of ultraviolet photolysis can be recognized by other characteristics such as the presence of radicals (e.g., HCO and H_2CO) and more complex molecules in the ices (i.e., aldehydes and ketones; Hagen, Allamandola, and Greenberg 1979; d'Hendecourt *et al.* 1986; Tielens *et al.* 1984, 1988). Unfortunately, published observations do not yet have high enough resolution and signal-to-noise ratio to realize the full potential of this spectral region.

c) *Astronomical Spectra in the Solid* CO *Spectral Region*

The 2200–2100 cm^{-1} (4.55–4.76 μm) observations of W33 A and NGC 7538–IRS 9 by Lacy *et al.* (1984) are most suited for a detailed analysis, both because of their relatively high resolution ($\lambda/\Delta\lambda \sim 850$) and the high optical depth of the absorption features detected in these sources ($\tau \sim 0.5$–2). These observations reveal the presence of three absorption com-

ponents with variable relative strengths in this wavelength region. They are (i) a narrow absorption at 2139.5 cm^{-1} (4.674 μm) with a width of about 5 cm^{-1}; (ii) a broader absorption on the wing of the 2139.5 cm^{-1} feature near 2134 cm^{-1} (4.686 μm) with a width of about 12 cm^{-1}; and (iii) a broader ($\Delta\nu = 28$ cm^{-1}) absorption at 2164.8 cm^{-1} (4.619 μm). The peak frequency and width of the second component is uncertain by several wavenumbers, due to overlap and blending with the (stronger) narrow component at 2139.5 cm^{-1}. There is some indication that the peak frequency of the narrow absorption feature may vary from source to source by perhaps as much as 0.8 cm^{-1}. Although observed at lower resolution ($\lambda/\Delta\lambda \sim 600$), other sources show evidence for two distinct components near 2140 cm^{-1} as well (Geballe 1986). Finally, some sources also show absorption by warm gas-phase CO in this wavelength region (Geballe 1986; Geballe and Wade 1985). The astronomical data pertaining to solid-state CO absorption bands are summarized in Table 4. The solid-state bands at 2140 and 2134 cm^{-1} in the astronomical spectra have been identified with absorption due to CO in icy interstellar grain mantles, while the band at 2165 cm^{-1} has been attributed to the C≡N stretching mode in a nitrile or, more likely, an isonitrile (Lacy *et al.* 1984; d'Hendecourt *et al.* 1986; Larson *et al.* 1985).

i) *The Broad CO Component*

The broad CO component at about 2134 cm^{-1} is assigned to absorption by CO molecules mixed at low concentration in molecular grain mantles. An analysis of the (almost) complete 5000–700 cm^{-1} (2–14 μm) spectra of several infrared objects, including W33 A and NGC 7538–IRS 9, shows that H_2O is the most abundant molecule in the ice in these sources (Tielens and Allamandola 1987*b*). Moreover, the peak position and shape of the 3250 cm^{-1} (3.08 μm) and 1650 cm^{-1} (6.06 μm) O—H stretching and deformation bands seen toward these sources (as well as most other observed sources) reveal that the H_2O molecules are organized in an almost complete hydrogen-bonding network. This implies that H_2O is the dominant species in these grain mantles (Hagen, Tielens, and Greenberg 1983). Both the observed band position and FWHM of the broad CO feature seen in the astronomical data are in reasonable agreement with an assignment to CO mixed in H_2O–rich ices (cf. Table 1). The broad, shallow 2152 cm^{-1} (4.647 μm) band accompanying the CO band in the spectra of laboratory H_2O ice mixtures at low temperatures ($T < 50$ K) is predicted to have an optical depth of less than 0.15 in these two sources. This feature is too small to be detected in the presently available astronomical spectra due to the low resolution of the observations, the overlap with the X:(C≡N) band at 2165 cm^{-1}, and the possible presence of interfering gas-phase CO lines. Thus the presently available observations cannot be used to constrain the thermal history of the grain mantles further. The presence of a large concentration ($\geq 10\%$) of nonpolar impurity molecules in the H_2O–rich ice mantles would increase the strength of the 2152 cm^{-1} band to detectable levels. One cannot exclude such a concentration since ultraviolet radiation and thermal annealing decrease the strength of this band. We note, however, that this upper limit is consistent with analyses of the 5000–700 cm^{-1} spectra of these two sources, which imply grain mantles consisting of H_2O and the polar species CH_3OH (2:1) with only traces of other molecules intermixed in the ice (Tielens and Allamandola 1987*b*).

TABLE 4

SUMMARY OF PEAK POSITIONS, FWHM, OPTICAL DEPTHS, AND COLUMN DENSITIES OF SOLID-STATE CO TOWARD EMBEDDED OBJECTS

Source Name	Peak Position (cm^{-1})	Optical Depth (τ)	FWHM (cm^{-1})	N(CO)-solid $\times 10^{-17}$ (molecules cm^{-2})	Note
W33 A					
Narrow	2139.1[a]	0.56	(5)(τ/2)	3.0	b
Broad	2134.8	0.58	(12)(τ/2)	4.4	b
NGC 7538/IRS 9					
Narrow	2139.9[a]	2.09	5.0 (τ/2)	11.0	b
Broad	2134.9	0.46	(12)(τ/2)	3.5	b
NGC 7538/IRS 1	2139.9[a]	0.24	3.5 (τ/2)	0.76	b
W3/IRS 5	2140[a]	0.20	4.6 (τ/2)	0.83	b
Elias 1	2135 ± 2	0.10	~10–20 (τ/2)	0.9	c
Elias 7	2135 ± 2	0.13	~12 (τ/2)	0.9	c
Elias 13	2136 ± 2	0.22	~10 (τ/2)	1.3	c
Elias 16	2141 ± 2[a]	0.96	~5 (τ/2)	4.5	c
Elias 18	2140 ± 2[d]	0.35	~11 (τ/2)	2.9	c
GL 2136	2137 ± 2	0.15	~7	0.62	e
OMC 2/IRS 3	2137 ± 2	0.10	~10	0.59	e
GL 490	2140 ± 2	0.15	~5	0.68	e
NGC 2024/IRS 2	2137 ± 2	0.35	7	1.4	e
GL 961	2137 ± 2	0.30	11	1.9	e
GL 989	2137 ± 2	0.35	9	1.9	e
Mon R2/IRS 2	2137 ± 2	0.30	9	1.6	e

[a] For these features, $A = 1.0 \times 10^{-17}$ cm molecule^{-1} for pure CO was used rather than $A = 1.7 \times 10^{-17}$ cm molecule^{-1}, the value for CO in water ice. This assumes that A(CO) in the less-polar ices is similar to A(CO) in CO.

[b] Lacy *et al.* 1984 [τ and FWHM reported, FWHM on a log (F_λ) scale, N(CO) calculated from their published integrated band areas].

[c] Whittet, Longmore, and McFadzean 1985 [τ reported, FWHM on a log (F_λ) scale estimated from published spectra].

[d] The peak positions of these features indicate that they are comprised of comparable amounts of the broad and narrow solid CO bands. N(CO) was determined by arbitrarily assuming that half the band area was due to the narrow component and half to the broad component.

[e] Geballe 1986 (τ reported, FWHM on an F_λ scale estimated from published spectra).

ii) *The Narrow CO Component*

We attribute the narrow (FWHM ~ 5 cm^{-1}) 2139.5 cm^{-1} (4.674 μm) band (most prominent in the spectrum of NGC 7538–IRS 9) to the C≡O stretching vibration in nonpolar, mixed molecular CO ices. Polar impurity molecules may be present in such mixtures at a level of 20% or less. Future higher resolution observations can provide better constraints on the impurity level of polar species. For example, the peak frequency of the H_2O–CO binary complex falls between 2142.5 to 2149.0 cm^{-1} (4.667–4.653 μm) and depends on the CO:H_2O concentration of the mixture (e.g., 10:1 versus 2:1 for the band positions given above; see Table 1, and Hagen and Tielens 1981). The observed narrow CO feature (particularly in NGC 7538–IRS 9), interpreted in light of the laboratory data, represents the first evidence for the presence of a grain mantle component dominated by molecules other than H_2O. One possibility is that the narrow CO component corresponds to icy grain mantles dominated by CO_2.

d) Solid-State CO Column Densities

In Table 4, infrared observations of interstellar CO bands have been compiled from the literature (Lacy *et al.* 1984; Geballe 1986; Whittet *et al.* 1985). For most sources the resolution was insufficient for a detailed decomposition of the CO feature into broad and narrow components. The features in the spectra of these sources have been somewhat arbitrarily divided into narrow and broad CO components (narrow corresponds to $\Delta\nu < 6$ cm^{-1}). It is important to use the appropriate A-values when determining the column density of CO in interstellar ices. If the observed band is broader than about 5 cm^{-1}, the A-value of CO in H_2O-rich ice of $A(CO)_{2137} = 1.7 \times 10^{-17}$ cm molecule^{-1} should be used. If, on the other hand, the FWHM of the band falls between 1 and 5 cm^{-1}, the A-value for pure CO ice of $A(CO)_{2139} = 1.0 \times 10^{-17}$ cm molecule^{-1} is appropriate. To date only a few objects have been observed which show such a narrow CO band in their spectra. Note that when the increased value of A(CO) for CO in H_2O-rich ice may be more appropriate, the previously inferred column densities for CO frozen in ices are reduced by a factor of about 0.60. Table 4 contains a summary of the column densities of solid-state CO for all previously published astronomical spectra using the corrected A(CO)-values given in Table 3. Note that entries have been omitted for the 11 objects, such as BN and OMC 1–IRC 2, that have been studied and exhibit no detectable solid-state CO feature (i.e., $\tau < 0.05$; Geballe 1986).

Comparing the CO column densities with typical H_2O column densities of 10^{18}–10^{19} cm^{-2} (Tielens *et al.* 1988) shows that, on the average, CO accounts for a few percent of the interstellar grain mantles (Tielens and Allamandola 1987*b*). This was the reason we used X:CO = 20:1 ices for the laboratory experiments where X represents the matrix species. Nevertheless, the presence of the narrow CO component in some lines of sight shows that the composition of interstellar grain mantles varies considerably from source to source and even along one line of sight. NGC 7538–IRS 9 is a particularly good example of the latter case (see Table 4) and will be discussed in more detail below.

e) The Solid-State CO Feature and Grain Surface Chemistry

The expected compositions of interstellar grain mantles have been calculated using theories that employ both gas phase and grain surface reactions (Tielens and Hagen 1982; Tielens 1983; d'Hendecourt, Allamandola and Greenberg 1985). Three distinct regimes, which depend on the composition of the gas phase, can be discerned from the results of these calculations (cf. Tielens and Allamandola 1987*a*). First, when atomic hydrogen is more abudant in the gas phase than the heavier species (e.g., CO, O, and O_2), the calculated grain mantle will be dominated by hydrogenated species such as H_2O, H_2CO, and possibly CH_3OH, while CO is only a trace constituent. Second, when atomic hydrogen is less abundant than the heavier species and most of the oxygen is in molecular form, few reactions will occur and the grain mantle will reflect the gas-phase composition. In this case, CO and O_2 are the dominant grain mantle species. Third, when atomic hydrogen is less abundant than the heavier species and atomic oxygen is present, the grain mantles may be enriched in CO_2. Although the surface reaction to produce CO_2 from CO and O may be inhibited at low temperatures (Grim and d'Hendecourt 1986), ultraviolet photolysis of these ices certainly produces CO_2 (cf. Fig. 6).

We will interpret the observation of the two distinct solid-state CO features (broad and narrow) in the astronomical spectra in terms of this trichotomy. The narrow CO component is then identified with grain mantles dominated by the direct accretion of nonpolar gas-phase species in an inert or oxidizing environment. In contrast, grain surface reactions have played an important role in determining the composition of the grain mantles responsible for the broad CO component.

The observation of superposed broad and narrow bands in the spectra of some interstellar clouds suggests that both types of environments can exist along one line of sight (Lacy *et al.* 1984). A case in point is provided by the spectrum of NGC 7538–IRS 9 (Fig. 7). Comparison of the abundance of ice components along the line of sight to this object shows that H_2O is the most abundant mantle species, suggesting that grain surface reactions have been important in much of this cloud. This conclusion is supported by the observation of the 1460 cm^{-1} (6.85 μm) absorption band in the spectrum of NGC 7538–IRS 9. This feature is attributed to simple alcohols like CH_3OH (methanol), which may result from grain surface reactions of CO with atomic hydrogen (Tielens and Hagen 1982; Tielens *et al.* 1988). Some of the solid CO along the line of sight is frozen in these H_2O-rich ices. This component produces a broad absorption at about 2134 cm^{-1} and is responsible for the low-frequency shoulder seen on the CO band of NGC 7538–IRS 9 (see Fig. 7).

However, the superposition of a narrow CO band demonstrates that there is a region along this line of sight in which the mantles are not dominated by H_2O, but are instead dominated by nonpolar species. As noted before, this suggests accretion of gas-phase species in an inert or oxidizing environment. Under these conditions the dominant ice material may be CO and O_2, or CO_2. Inspection of Figure 7 and Table 1 shows that the band produced by CO in O_2-rich ice fails to match the narrow interstellar feature in both position and width. The band produced by pure CO ice is also too narrow and, while falling about 2 cm^{-1} closer to the interstellar band position than does CO in O_2, it still does not match the observed position. CO in CO_2-rich ices, however, provides a reasonably good fit to both position and profile. Photolysis of pure CO might result in a wider feature but is unlikely to produce the required band shift. In any event, the photolysis of pure CO ice undoubtedly results in the production of CO_2, and we are returned to the conclusion that CO_2 is likely to be involved. Thus we suggest that the

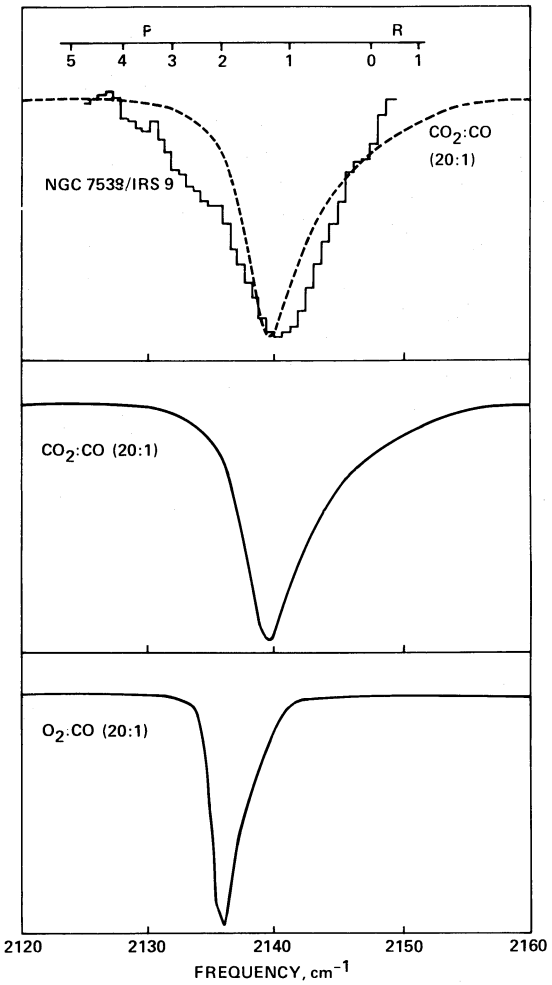

FIG. 7.—The infrared spectrum of the solid CO feature in NGC 7538–IRS 9 (top, reproduced from Lacy *et al.* 1984) compared to the bands produced by CO in CO_2:CO = 20:1 (*middle*) and O_2:CO = 20:1 (*bottom*) ices. The dashed line in the NGC 7538–IRS 9 spectrum is that of the CO_2:CO ice. Note that the CO_2–rich ice provides a good fit to the narrow component of the astronomical data, while the O_2–rich ice does not. The low-frequency shoulder at about 2134 cm^{-1} on the NGC 7538–IRS 9 feature is due to an additional component along the line of sight in which the CO is intimately mixed in H_2O–rich ices (see text). The numbered lines above the top spectrum denote the positions of the rotational lines of gas-phase CO which may contribute to some of the absorption.

narrow CO band in NGC 7538–IRS 9 may be due to CO frozen in CO_2–rich ices. Finally, we note that CO_2 (which is undetectable from the ground and airborne altitudes) could well be more abundant than H_2O along the line of sight to this object.

V. SUMMARY

We have presented the results of laboratory work in which we investigated the infrared spectral properties of CO in over 55 ice mixtures. Detailed examination of the C≡O stretching fundamental band near 2137 cm^{-1} shows that the exact position, FWHM, and profile of the band severely constrains the conditions under which the ice formed and its subsequent thermal and radiation exposure history.

Ices in which H_2O is the dominant component trap CO in two distinct molecular sites, resulting in an additional absorption band near 2152 cm^{-1}. The frequency of this new band suggests that the additional site is "repulsive" and may be interstitial. Evidence of this band in the spectra of astronomical infrared sources containing H_2O–rich ices has not yet been found since the strength of this feature falls below the detection limits of past studies. The present "nondetection" of the 2152 cm^{-1} band in the astronomical spectra implies, however, that either the abundance of nonpolar impurities (like aliphatic hydrocarbons) in the mantles must be less than 10%, or that they have been thermally annealed or processed by ultraviolet radiation.

Comparison of the laboratory data with astronomical spectra shows that the composition of interstellar ice mantles varies considerably from source to source. In most sources the CO is intimately mixed in ices dominated by polar molecules, of which H_2O is probably the major component. There is evidence, however, that a component of the solid CO in some sources (such as NGC 7538–IRS 9) is condensed in nearly pure form or is incorporated into ices dominated by other nonpolar molecules. Spectral matches suggest that CO_2–rich ices may be responsible. The compositional differences suggested by the spectra can be understood in terms of differences between the relative gas-phase abundances of atomic versus molecular hydrogen and the presence of hydrogenated versus nonhydrogenated species (such as CO, O, and O_2) during the formation of the ice mantles.

Determination of the absorption coefficient of the CO fundamental band for CO in H_2O–rich ices showed that the previously used A(CO)-values (applicable only to pure CO ices) were approximately 60% too low and previously estimated interstellar column densities should be decreased accordingly.

We also note that careful observation of the solid-state ^{13}CO and ^{12}CO bands at 2090 and 2137 cm^{-1}, respectively, can potentially provide information on the $^{13}C/^{12}C$ ratio in astrophysical ices.

In conclusion, analysis of high-quality data in the 2200–2100 cm^{-1} infrared spectral region of the C≡O fundamental stretching vibration can provide a wealth of detailed information about astrophysical ices. Clearly, a great deal of additional work in this spectral region is merited.

The authors would like to thank Tom Geballe and an anonymous referee for helpful comments and suggestions resulting in an improved version of this paper.

REFERENCES

Allamandola, L. J. 1984, in *Galactic and Extragalactic IR Spectroscopy*, ed. M. Kessler and P. Phillips (Dordrecht: Reidel), p. 5.
Allamandola, L. J., Sandford, S. A., and Valero, G. J. 1988, *Icarus*, submitted.
Barnes, A. G. 1973, in *Vibrational Spectroscopy of Trapped Species*, ed. H. E. Hallam (New York: Wiley), p. 133.
Behringer, R. E. 1958, *J. Chem. Phys.*, **29**, 537.
Bertie, J. E., Labbe, H. J., and Whalley, E. 1969, *J. Chem. Phys.*, **50**, 4501.
d'Hendecourt, L. B., and Allamandola, L. J. 1986, *Astr. Ap. Suppl.*, **64**, 453.
d'Hendecourt, L. B., Allamandola, L. J., and Greenberg, J. M. 1985, *Astr. Ap.*, **152**, 130.
d'Hendecourt, L. B., Allamandola, L. J., Grim, R. J. A., and Greenberg, J. M. 1986, *Astr. Ap.*, **158**, 119.
Dubost, H. 1976, *Chem. Phys.*, **12**, 139.
Dubost, H., and Abouaf-Marguin, L. 1972, *Chem. Phys. Letters*, **17**, 269.
Ewing, G. E., and Pimentel, G. C. 1961, *J. Chem. Phys.*, **35**, 925.
Geballe, T. R. 1986, *Astr. Ap.*, **162**, 248.

Geballe, T. R., and Wade, R. 1985, *Ap. J.* (*Letters*), **291**, L55.
Grim, R. J. A., and d'Hendecourt, L. B. 1986, *Astr. Ap.*, **167**, 161.
Hagen, W., Allamandola, L. J., and Greenberg, J. M. 1979, *Ap. Space Sci.*, **65**, 215.
———. 1980, *Astr. Ap.*, **86**, L3.
Hagen, W., and Tielens, A. G. G. M. 1981, *J. Chem. Phys.*, **75**, 4198.
Hagen, W., Tielens, A. G. G. M., and Greenberg, J. M. 1981, *Chem. Phys.*, **56**, 367.
———. 1983, *Astr. Ap. Suppl.*, **51**, 389.
Huheey, J. E. 1983, *Inorganic Chemistry*, (3d ed.; New York: Harper and Row), p. 141.
Jiang, G. J., Person, W. B., and Brown, K. G. 1975, *J. Chem. Phys.*, **62**, 1201.
Kitta, K., and Kratschmer, W. 1983, *Astr. Ap.*, **122**, 105.
Lacy, J. H., Baas, F., Allamandola, L. J., Persson, S. E., McGregor, P. S., Lonsdale, C. J., Geballe, T. R., and van de Bult, C. E. P. 1984, *Ap. J.*, **276**, 533.
Larson, H. P., Davis, D. S., Black, J. H., and Fink, U. 1985, *Ap. J.*, **299**, 873.
Legay-Sommaire, N., and Legay, F. 1982, *Chem. Phys.*, **66**, 315.
Leger, A., Gauthier, S., Defourneau, D., and Rouan, D. 1983, *Astr. Ap.*, **117**, 164.
Sandford, S. A., and Allamandola, L. J. 1988, *Icarus*, submitted.
Soifer, B. T., Puetter, R. C., Russell, R. W., Willner, S. P., Harvey, P. M., and Gillett, F. C. 1979, *Ap. J.* (*Letters*), **232**, L53.
Tarafdar, S. P., and Vardya, M. S., eds. 1987, *IAU Symposium 120, Astrochemistry* (Dordrecht: Reidel), in press.
Tielens, A. G. G. M. 1983, *Astr. Ap.*, **119**, 117.
Tielens, A. G. G. M., and Allamandola, L. J. 1987*a*, in *Interstellar Processes*, ed. D. Hollenbach and H. Thronson (Dordrecht: Reidel), p. 397.
———. 1987*b*, in *Physical Processes in the Interstellar Medium*, ed. G. E. Morfill and M. Scholer (Dordrecht: Reidel), p. 333.
Tielens, A. G. G. M., Allamandola, L. J., Bregman, J., Goebel, J., d'Hendecourt, L. B., and Witteborn, F. 1984, *Ap. J.*, **287**, 697.
Tielens, A. G. G. M., Allamandola, L. J., Bregman, J. D., Witteborn, F. C., Wooden, D., and Rank, D. M. 1988, *Ap. J.*, in preparation.
Tielens, A. G. G. M., and Hagen, W. 1982, *Astr. Ap.*, **114**, 245.
van Dishoek, E., and Black, J. H. 1987, in *Physical Processes in the Interstellar Medium*, ed. G. E. Morfill and M. Scholer (Dordrecht: Reidel), p. 241.
Whittet, D. C. B., Longmore, A. J., and McFadzean, A. D. 1985, *M.N.R.A.S.*, **216**, 45P.
Wilson, R. W., Jefferts, K. B., and Penzias, A. A. 1971, *Ap. J.* (*Letters*), **161**, L43.
Wood, B. E., and Roux, J. A. 1982, *J. Opt. Soc. America*, **72**, 720.

LOUIS J. ALLAMANDOLA, SCOTT A. SANDFORD, A. G. G. M. TIELENS, and GUSTAVO J. VALERO: NASA/Ames Research Center, Mail Stop 245-6, Moffett Field, CA 94035